MAGNETIC SWITCHING

Many applications of ferromagnetic materials are based on the fact that the magnetization can move from one stable state (direction) to another stable state. Ferromagnetic materials, like ferrimagnetic materials, possess spontaneous magnetic polarization in the absence of an applied field. The manner in which the magnetization changes, together with the time necessary for completing the magnetization state change, is of primary significance. A directional change in magnetization state can be thermally activated or result from applying an external magnetic field. The process of changing the magnetization direction is called magnetization switching or reversal. The magnetic switching process is extremely complex, because it is inherently nonlinear and depends nontrivially on material properties, magnetic structure, magnetic history, specimen geometry, amplitude and direction of the applied switching magnetic field, damping mechanisms, and switching-field time dependence. This article addresses the physical phenomenology involved in magnetic switching and is organized as follows:

J. Webster (ed.), *Wiley Encyclopedia of Electrical and Electronics Engineering*.

- Magnetic moments (phenomenological and atomic models, interactions with applied static and frequency-dependent magnetic fields, magnetization equations of motion, resonance, magnetic susceptibility, dipole interaction energy, orbital and spin moments)
- Magnetic domains (general structure; magnetocrystalline anisotropy, exchange, magnetostatic, and magnetostriction energy; Bloch walls and Néel walls)
- Magnetic switching analysis (quasi-static and dynamic, single and multiple domains, coherent and incoherent rotation, damping mechanisms, hysteresis, giant magnetoresistance, spin valves)

MAGNETIC MOMENTS

Magnetic moments can be understood by phenomenological or atomic models. An elementary model is the magnetic dipole in which magnetic moments are described in terms of *equivalent* opposite magnetic charges separated by a distance d whose product yields the magnetic dipole moment $\boldsymbol{m}_\mathrm{d}$. This model is analogous to that of an electric dipole moment of a pair of charges, $-q$ and $+q$, separated by a distance d. An equivalent phenomenological model is given in terms of a conventional current I flowing in a closed loop of area A [Fig. 1(a)], which has a magnetic dipole moment amplitude $m_\mathrm{d} = IA$. The interaction of a magnetic dipole with an externally applied field $\boldsymbol{H}_0$ is given by the torque imposed on the dipole in the presence of the applied field:

$$\begin{aligned}\boldsymbol{T}_\mathrm{d} &= \mu_0 \boldsymbol{m}_\mathrm{d} \times \boldsymbol{H}_0 \\ &= -\mu_0 m_\mathrm{d} H_0 \sin\theta\end{aligned} \tag{1}$$

where μ_0 is the magnetic permeability of vacuum ($4\pi \times 10^{-7}$ H/m), θ is the angle between the dipole axis and the externally applied field, and the sign is chosen so that T_d is a restoring torque [Fig. 1(b)]. The angular gradient of the interaction (potential) energy between the magnetic dipole and the external field also represents the torque exerted on the dipole. The interaction energy E is given by

$$E = -\mu_0 m_\mathrm{d} H_0 \cos\theta \tag{2}$$

and

$$T_\mathrm{d} = -\frac{\partial E}{\partial \theta} \tag{3}$$

In an applied field, the dipole has minimum energy ($-\mu_0 m_\mathrm{d} H_0$) at $\theta = 0$ and increases as the dipole moment is turned away from $\boldsymbol{H}_0$. At $\theta = \pi$, the dipole is in unstable equilibrium. The fundamental equation of motion of a magnetic dipole in an external field is derived from the torque equation because the torque is the gradient with respect to time of the angular momentum $\boldsymbol{L}_\mathrm{d}$ of the dipole. The magnetic dipole moment $\boldsymbol{m}_\mathrm{d}$ may be written as

$$\boldsymbol{m}_\mathrm{d} = \gamma' \boldsymbol{L}_\mathrm{d} \tag{4}$$

where $\gamma' = m_\mathrm{d}/L_\mathrm{d}$. For a single electron moving in a circle, γ' is given by $e/(2m_\mathrm{e})$, where e and m_e are the charge and mass of the electron. The torque may be written

$$\begin{aligned}\boldsymbol{T}_\mathrm{d} &= \frac{d\boldsymbol{L}_\mathrm{d}}{dt} \\ &= \mu_0 \boldsymbol{m}_\mathrm{d} \times \boldsymbol{H}_0\end{aligned} \tag{5}$$

or, equivalently, the equation of motion of the magnetic dipole in an applied field $\boldsymbol{H}_0$ is

$$\begin{aligned}\frac{d\boldsymbol{m}_\mathrm{d}}{dt} &= \mu_0 \gamma' \boldsymbol{m}_\mathrm{d} \times \boldsymbol{H}_0 \\ &= \gamma_\mathrm{c} \boldsymbol{m}_\mathrm{d} \times \boldsymbol{H}_0\end{aligned} \tag{6}$$

where $\gamma_\mathrm{c} = \mu_0 \gamma'$ is the gyromagnetic ratio of a circulating charge (neglecting spin). Because of spin and angular momentum in a real magnetic ion, γ_ion can differ significantly from $\mu_0 e/(2m_\mathrm{e})$. In fact, a magnetic material may contain several magnetic ions so that its effective gyromagnetic ratio γ_eff differs from those of the individual ionic species present.

It is useful to review the effects of a static field and a frequency-dependent field on the equation of motion for a simple magnetic dipole. Time-dependent equations of magnetization motion, which will be addressed later in this chapter, can be derived from inverse Fourier transforms of frequency-domain expressions. In addition, specific details of individual magnetic fields comprising the net *effective* field acting on the time-dependent magnetization vector in a ferromagnetic medium may be better understood.

If the total external applied magnetic field is written as the sum of a static field $\boldsymbol{H}_0$ and a frequency-dependent field $\boldsymbol{h}e^{j\omega t}$, where $\omega = 2\pi f$ is the angular frequency,

$$\boldsymbol{H}(t) = \boldsymbol{H}_0 + \boldsymbol{h}e^{j\omega t} \tag{7}$$

the time-harmonic case may be examined. Equation (7) may be substituted in Eq. (6) to give the *magnetic susceptibility* tensor relating the applied static external magnetic field, the components of magnetization, and the frequency-dependent field transverse to $\boldsymbol{H}_0$. Their dependence on the frequency ω,

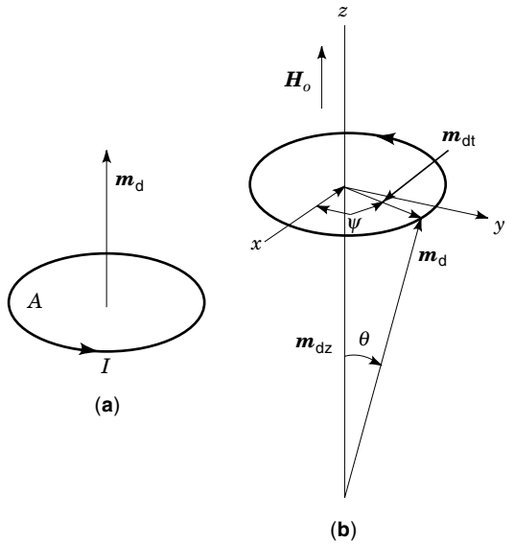

Figure 1. Magnetic dipole moment of circulating charge (a) and interaction of dipole with external magnetic field (b).

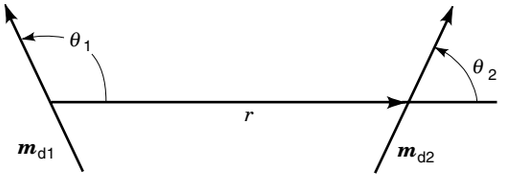

Figure 2. Interaction of two magnetic dipoles in the same plane oriented at arbitrary angles to a position vector separating them.

and the *Larmor* precessional frequency, $\omega_0 = d\psi/dt = |\gamma|H_0$, can also be derived. The phenomenological model is illustrated in Fig. 1(b). Allow the direction of $\boldsymbol{H}_0$ to be along the z-axis, so that

$$\boldsymbol{H} = H_0\hat{a}_z + (h_x\hat{a}_x + h_y\hat{a}_y + h_z\hat{a}_z)e^{j\omega t} \tag{8}$$

If $|\boldsymbol{h}| \ll |\boldsymbol{H}_0|$, then $|\boldsymbol{m}_{dt}| \ll |\boldsymbol{m}_{dz}|$ and

$$\boldsymbol{H} = \begin{bmatrix} h_x \\ h_y \\ H_0 \end{bmatrix}, \quad \boldsymbol{m}_d = \begin{bmatrix} m_{dx} \\ m_{dy} \\ m_{dz} \end{bmatrix} \tag{9}$$

where $\boldsymbol{m}_d = \boldsymbol{m}_{dt} + m_{dz}\hat{a}_z$, $\boldsymbol{m}_{dt} = m_{dx}\hat{a}_x + m_{dy}\hat{a}_y$ and $m_{dz} \simeq m_d$. The equation of motion of the magnetic dipole of moment m_d yields

$$\begin{bmatrix} m_{dx} \\ m_{dy} \\ m_{dz} \end{bmatrix} = \begin{bmatrix} \gamma^2 m_d H_0/(\gamma^2 H_0^2 - \omega^2) & -j\omega\gamma m_d/(\gamma^2 H_0^2 - \omega^2) & 0 \\ j\omega\gamma m_d/(\gamma^2 H_0^2 - \omega^2) & \gamma^2 m_d H_0/(\gamma^2 H_0^2 - \omega^2) & 0 \\ 0 & 0 & 0 \end{bmatrix} \begin{bmatrix} h_x \\ h_y \\ H_0 \end{bmatrix} \tag{10}$$

This may be simply written

$$\boldsymbol{m}_d = [\chi] \cdot \boldsymbol{H} \tag{11}$$

where $[\chi]$ is the classical Polder magnetic susceptibility tensor without damping. The magnetic permeability is $[\mu] = [1] + [\chi]$ where [1] is the unit tensor. Equation (10) gives a resonant condition when $\omega = |\gamma| H_0$, and shows that the components of the magnetic dipole moment depend on the orientation of the field $\boldsymbol{H}$. Equation (10) represents a *steady-state* solution for the magnetic dipole in an applied field $\boldsymbol{H}$. Other frequency-domain expressions can be derived that correspond to various transient excitations.

Dipole–Dipole Interactions

The interaction of dipole moments influences the equations of motion of magnetization. One simple case is the general configuration of two dipoles that have magnetic moments $\boldsymbol{m}_{d1}$ and $\boldsymbol{m}_{d2}$ illustrated in Fig. 2. The dipole–dipole interaction energy is given by

$$E = \frac{\mu_0 \boldsymbol{m}_{d1} \cdot \boldsymbol{m}_{d2}}{r^3} - \frac{3\mu_0 (\boldsymbol{m}_{d1} \cdot \boldsymbol{r})(\boldsymbol{m}_{d2} \cdot \boldsymbol{r})}{r^5} \tag{12}$$

where $\boldsymbol{r}$ is the position vector from dipole 1 to dipole 2. In a ferromagnetic material, $\boldsymbol{m}_{d1} = \boldsymbol{m}_{d2} = \boldsymbol{m}_d$ and are parallel, so the interaction energy becomes

$$E = \frac{\mu_0 m_d^2}{r^3}(1 - 3\cos^2\theta) \tag{13}$$

If the dipole moments are parallel to the position vector [Fig. 3(a)] and are rotated through an angle θ from the z-axis [Fig. 3(b)], there is a restoring torque in addition to the torque from any external field. The restoring torque is represented by

$$\begin{aligned} T &= -\frac{\partial E}{\partial \theta} \\ &= -2\mu_0 m_d \left(\frac{3m_d}{r^3}\cos\theta\right)\sin\theta \\ &= -\mu_0 M_d H_{Dz}\sin\theta \end{aligned} \tag{14}$$

where $M_d = 2m_d$ and H_{Dz} is an apparent field in the z-direction, that is,

$$H_{Dz} = \frac{3M_{dz}}{2r^3} = DM_{dz} \tag{15}$$

where $M_{dz} = M_d \cos\theta$.

Then the magnetization equation of motion of two aligned magnetic dipoles in an external field $\boldsymbol{H}_0$ becomes

$$\frac{d\boldsymbol{M}_d}{dt} = \gamma \boldsymbol{M}_d \times (\boldsymbol{H}_0 + \boldsymbol{H}_D) \tag{16}$$

If $\boldsymbol{H}_0$ is directed along the z-axis, the time derivatives of the transverse components of the total magnetization vector become

$$\begin{aligned} \frac{dM_{dx}}{dt} &= \gamma[M_{dy}H_0 - M_{dz}(-DM_{dy})] \\ \frac{dM_{dy}}{dt} &= \gamma[M_{dz}(-DM_{dx}) - M_{dx}H_0] \end{aligned} \tag{17}$$

Similar equations can be written when magnetic dipoles are parallel but normal to the position vector connecting them. In this case, for an applied field $\boldsymbol{H}_0$ in the y-direction

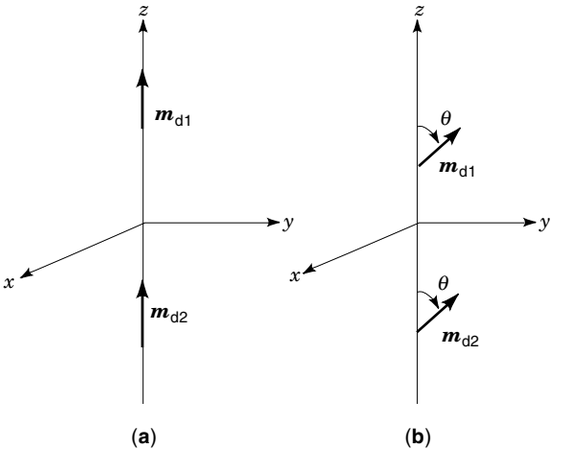

Figure 3. Aligned magnetic dipoles parallel to a position vector separating them (a) and rotational angle θ causing restoring torque (b).

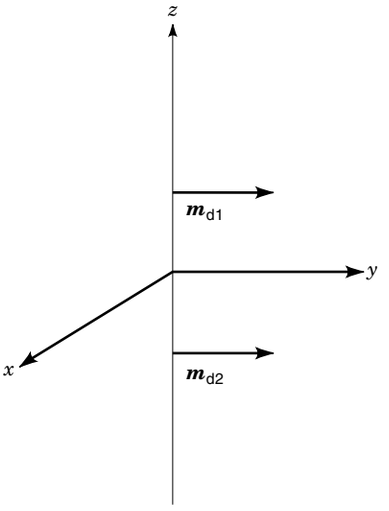

Figure 4. Aligned magnetic dipoles normal to a position vector separating them.

(see Fig. 4), the equations of motion of the resultant magnetization are

$$\begin{aligned}\frac{dM_{dx}}{dt} &= \gamma[-M_{dz}(H_0 - DM_{dy})] \\ \frac{dM_{dz}}{dt} &= \gamma[M_{dx}(H_0 - DM_{dy}) - M_{dy}(-DM_{dx})]\end{aligned} \tag{18}$$

Both Eqs. (17) and (18) have the general form

$$\begin{aligned}\frac{d\boldsymbol{M}_d}{dt} &= \gamma \boldsymbol{M}_d \times \left(\boldsymbol{H}_0 - \begin{bmatrix} D & 0 & 0 \\ 0 & D & 0 \\ 0 & 0 & 0 \end{bmatrix} \boldsymbol{M}_d \right) \\ &= \gamma \boldsymbol{M}_d \times (\boldsymbol{H}_0 - [D]\boldsymbol{M}_d)\end{aligned} \tag{19}$$

where $\boldsymbol{H}(t) = \boldsymbol{H}_0 - [D]\boldsymbol{M}_d$ is an internal *effective* field and $[D]$ is the two-dipole analog of the *demagnetization* tensor. Similar magnetization equations of motion for many-dipole arrays may be derived to gain insight into magnetic dipole alignment in an external magnetic field. However, dipole forces in solids are too weak to account for the large interaction energies that maintain alignment between a distribution of magnetic moments. These forces result from electron exchange, are quantum mechanical in origin, and must be understood in terms of the electron orbital and spin states of a magnetic ion.

Microscopic moments originate in very definite magnetic ions, elements of the periodic table. These ions are from one of two transition series that have an incomplete inner shell. The first transition series is that where the 3*d* electron shell is incomplete and consists of the elements ranging from calcium (atomic number 20) to zinc (atomic number 30). The second is the rare-earth series with an incomplete 4*f* shell. This contains elements 57 (lanthanum) through 71 (lutecium). The magnetic moments and angular momenta of all of the electrons occupying either the 3*d* or 4*f* shells combine to give a resultant magnetic moment of the ion.

The overall orbital angular momentum of a magnetic ion is specified by the quantum number L. In the presence of a magnetic field, a free magnetic ion with orbital quantum number L may only have specific discrete values of angular momentum which are integral multiples of $\hbar = h/(2\pi)$, where h is Planck's constant (6.625×10^{-34} J · s). So the associated orbital magnetic moment is given by

$$\begin{aligned}m_{dL} &= \gamma L\hbar \\ &= \mu_0 e\hbar L/(2m_e)\end{aligned} \tag{20}$$

Electron spin also gives rise to a magnetic moment. However, in this case, the magnetomechanical ratio $\gamma_{spin} = 2\gamma$, and the magnetic moment due to spin is given by

$$m_{dS} = 2\gamma S\hbar \tag{21}$$

where S is the spin quantum number. Neighboring ions affect the net orbital angular momentum. For elements of the first transition series, orbital angular momentum and associated magnetic moment are almost completely destroyed by electrostatic interactions with the lattice environment. The orbital contributions for the rare-earth series are also disturbed by neighboring ions but to a lesser extent. Therefore, for the first transition series of elements, the overall magnetic moment is close to that given by Eq. (21), so that the general form of the gyromagnetic ratio is

$$\gamma = \frac{g\mu_0 e}{(2m_e)}, \tag{22}$$

where g is the Lande spectroscopic splitting factor ($g = 2.0023$ for a free electron). The value of $|\gamma|$ is 2.2×10^5 rad · m/(A · s).

MAGNETIC DOMAINS

Magnetic reversal, permeability, and hysteresis all depend on the structure of the magnetic domain and the variability of this structure under the effect of an applied external field. There are two general approaches for magnetization analysis. One approach, first introduced by Weiss (1) in 1907, is based on experimental evidence of the spatial distribution of magnetization in magnetic domains. Another approach, proposed by Brown (2), is based on the assumption that the magnetic polarization is a function of coordinates of the point at which it is being evaluated. In the Weiss model, each magnetic domain has a spontaneous, generally uniform, magnetic polarization density I_s oriented differently from those of its neighbors (see Fig. 5). The different *magnetic domains* or *Weiss domains* are separated by transition zones called *Bloch walls.* The atomic magnetic moments within each domain are aligned parallel to each other and across the Bloch wall the magnetic moments rotate to that in a neighboring domain. This rotation is illustrated for a 180° Bloch wall in Fig. 6. Thus the parallel orientation of magnetic moments is a *local* phenomenon. Several experimental techniques make it possible to show the distribution of magnetic polarization in a specimen.

One of the first experiments for observing magnetic domain walls in a bulk ferromagnetic specimen was performed by Barkhausen in 1919. In Barkhausen's experiment, a permanent magnet was rotated slowly with an approximate period of one second about a solenoidal winding holding a ferromagnetic rod specimen. The winding around the specimen detected variations in magnetic flux that were transmitted

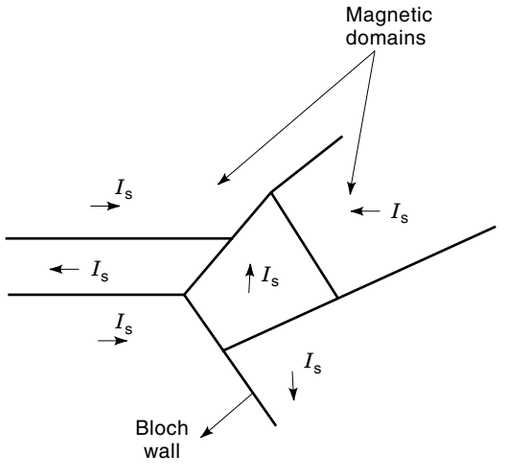

Figure 5. The magnetic domain structure of a specimen showing magnetic polarization $\boldsymbol{I}_s$ within each domain.

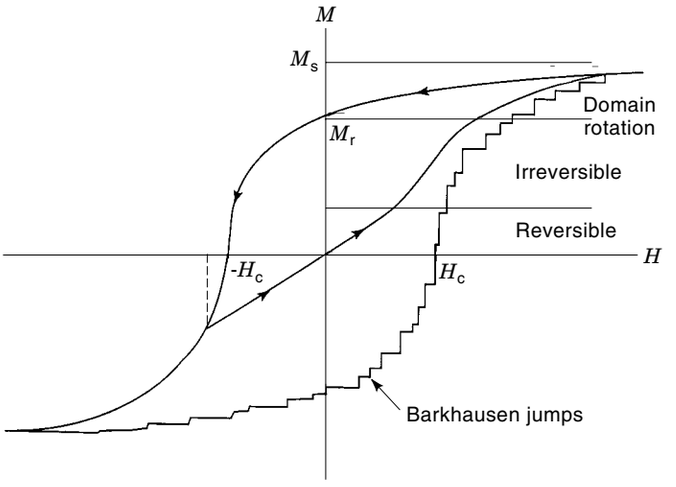

Figure 7. Magnetization loop characteristics showing Barkhausen's jumps from domain wall movements. M is magnetization as a function of applied magnetic field H. M_s, M_r are saturation and remanent magnetizations. H_c is intrinsic coercive field.

after amplification to a loudspeaker. Each time the polarization was reversed, audible sounds reflecting small magnetic grain deformation could be heard. The change in polarization of the ferromagnetic rod occurs in small successive steps, now known to correspond to the sudden change of *pinning points* on the Bloch walls (see Fig. 7). Pinning points, or points that fix or retain Bloch wall structure, are principally caused by various kinds of specimen inhomogeneity rather than specimen size or shape. The types of inhomogeneity affecting domain structure are voids, inclusions, fluctuations in alloy composition, local internal stresses, and the local directional order of crystal boundaries. Figure 7 illustrates the typical appearance of a *magnetic hysteretic* loop, which results from irreversible changes in magnetization that cause dissipation in the form of heat in the specimen. The *coercivity* or coercive field H_c is that magnetic field that must be applied in the opposite direction to restore zero magnetization. The area enclosed by the hysteretic loop is proportional to the energy dissipated into heat for each cycle around the loop. The coercive field is the ultimate determining factor for magnetic switching energy, which is approximately equal to the product of $2H_c$ and the remanent magnetization M_r. The coercive field also limits the minimum drive field required for domain switching. Another important parameter of the hysteretic loop for switching performance is the *squareness ratio* defined by M_r/M_s. Better switching performance is obtained when the squareness ratio has a value close to one. Irreversible changes in magnetization are addressed in the Preisach model for magnetic switching analysis of multiple-domain particles.

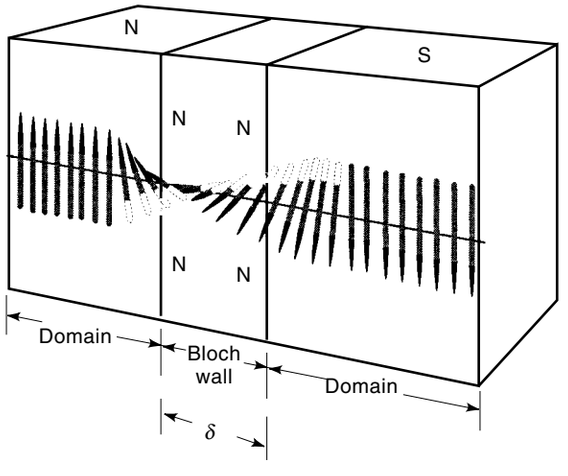

Figure 6. The magnetic structure of a Bloch wall of thickness δ separating 180° domains (6).

Another technique for observing magnetic domains directly is the Bitter method. The Bitter method consists of spreading a colloidal solution of magnetic particles on the surface of a specimen that has been electrolytically polished. Upon evaporation of the solvent, magnetic flux leakage occurs where the Bloch walls intersect the surface of the specimen. The leakage produces an accumulation of magnetic particles that can be observed with a microscope and which define the Bloch walls. Other methods that permit observing Bloch walls in movement are based on the rotation of the polarization of linearly polarized light during transmission (the *Faraday effect*) or during reflection (the *Kerr effect*). High-quality optical systems must be used to observe the small angles of polarization rotation in the last two methods.

Recently, magnetic force microscopy (MFM) has been used to image magnetic domain wall structures. The divergence of the magnetization in the walls is reflected by fringing magnetic fields outside the specimen. The magnetostatic interaction between the magnetic specimen and a magnetic sensor is measured. The sensor is a sharp tip coated with a magnetic thin film at the end of a flexible cantilever. When the tip is positioned a sufficient distance (typically 50 to 150 nm) away from the specimen surface, the cantilever responds to magnetic force gradients acting on the tip. MFM data permit high resolution, high sensitivity imaging of magnetic domains and other micromagnetic structures.

Magnetic domains can have highly variable shapes. A simple model for the modulus of the spontaneous polarization density vector $\boldsymbol{I}_s$ is that it has the same value in all domains

of a homogeneous material, provided that the temperature distribution is uniform. The magnetic moment $\boldsymbol{M}$ of a specimen of volume V must lie between the limits

$$0 \leq \boldsymbol{M} = \int_V \boldsymbol{I}_s dv \leq \boldsymbol{I}_s V \tag{23}$$

Hence the magnetic moment can vary from 0 to $\boldsymbol{I}_s V$ with an applied field H_0, which modifies the number, shape, and distribution of magnetic domains in the specimen.

General Structure of Magnetic Domains: Energy Considerations

Magnetic domain structures in either bulk or thin-film materials are expressed as statistical averages in terms of their size, shape, and internal orientation of the polarization vector $\boldsymbol{I}_s$. Only those structures are permissible in which a *local,* not *absolute* minimum in internal magnetic energy occurs. The internal energy E_i associated with magnetic domain structure is the sum of the magnetic anisotropy energy E_a, the exchange energy E_{ex}, the magnetostatic energy E_{ms}, and the magnetostriction energy E_{mt}.

Magnetocrystalline Anisotropy Energy. The interaction of atomic magnetic moments that leads to their parallel alignment is measured in terms of energy. In a crystal, a part of this energy, called the magnetocrystalline anisotropy energy, is a function of the angles that the magnetic moments have with respect to the crystal's axial directions. In a ferromagnetic crystal there are *easy* and *hard* directions of magnetization. In other words, the energy required to magnetize the crystal depends on the direction of the applied magnetic field relative to the crystalline axes. For single-crystal materials, such as iron, nickel, and their alloys, the anisotropy has cubic symmetry, provided they are prepared in the absence of a magnetic field. For crystals prepared or deposited in the presence of a magnetic field, a uniaxial symmetry is developed. A polycrystalline specimen of iron, nickel, or their alloys appears isotropic because of the random orientation of the constituent cubic crystallites.

The difference between the energies required to magnetize a crystal in the hard and easy directions is called the *anisotropy energy.* The magnetic anisotropy energy $E_a(\alpha_1, \alpha_2, \alpha_3)$, where α_1, α_2, α_3 are the directional cosines that the magnetic polarization vector makes with the crystal axes, varies in different materials (4,5). If only magnetic anisotropy energy is taken into account, spontaneous magnetic polarization in a crystal specimen generally aligns itself parallel to principal crystallographic planes that can be described by their *Miller indices.* In these directions E_a has local minima in which there are *easy magnetization directions.* In general, the anisotropy energy of cubic metals, such as iron or nickel, may be expressed in terms of the anisotropy energy E that has the form (3)

$$E_a = E_0 + E_1 + E_2 \tag{24}$$

where E_0 is purely isotropic and $E_1 = K_1(\alpha_1^2\alpha_2^2 + \alpha_2^2\alpha_3^2 + \alpha_3^2\alpha_1^2)$ and $E_2 = K_2\alpha_1^2\alpha_2^2\alpha_3^2$ are anisotropic. The constants K_1 and K_2 are the first- and second-order anisotropy constants that arise from interaction between the orbital angular momentum and the crystalline lattice and are usually determined by fitting experimental data. In the case of a uniaxial material, the anisotropy energy E_{ua} is given, to the first order, by $E_{ua} = K_u(1 - \alpha_z^2) = K_u \sin^2 \theta$, where K_u is the first-order uniaxial anisotropy constant. E_{ua} is independent of the azimuthal angle.

Generally, coercive fields increase monotonically with $|K_1|$ because of higher domain-wall energies and stronger pinning of domain walls at voids, inclusions, and fluctuations in ferromagnetic material composition. Where frequent and rapid switching of the magnetic state is required, materials are chosen that have small first-order anisotropy constants and low domain-wall energies.

Exchange Energy. Exchange energy takes into account the interaction between the atomic magnetic moments. This interaction can be understood only in terms of quantum-mechanical exchange integrals, which have no classical analogs. The exchange energy of an assembly of spins S is given by

$$E_{ex} = -2 \sum_{i,j} J_{ij} \boldsymbol{S}_i \cdot \boldsymbol{S}_j \tag{25}$$

where the subscripts i,j distinguish two atoms with different spin quantum numbers S_i and S_j which are given in terms of $\hbar = h/(2\pi)$, J_{ij} is the exchange integral that has dimensions of energy, and the sum represents the total exchange energy of all atomic spins in the specimen. The spin quantum numbers S_i and S_j are always multiples of 1/2 and are related to the atomic magnetic moments by $m = 2Sm_B$, where m_B is the Bohr magneton, that is, the magnetic moment of electron spin, $9.273 \cdot 10^{-24}$ A $\cdot$ m^2. The ground state for a ferromagnetic assembly has all spins parallel, so that the exchange integral J_{ij} is positive. If the spins vary from point to point (as in a ferrimagnetic specimen), then J_{ij} is negative, and the exchange energy is increased above its maximum negative value. In general, both the magnetocrystalline anisotropy and exchange energies increase inside a domain wall. The sum of the anisotropy and exchange energies usually characterizes the energy associated with the domain wall itself and can be used to approximate the thickness of the domain wall. However, the domain-wall energy limits the area of the wall because the magnetostatic energy due to demagnetization decreases in direct proportion to the number of domains formed. The actual number of domains formed in a specimen stabilizes when the reduction of magnetostatic energy is compensated by the increase in domain-wall energy due to anisotropy and exchange. Again, the *total* energy must be a local minimum.

The domain-wall energy per unit area U_{wall} for a planar domain wall in a bulk specimen that has average anisotropy energy per unit volume $\overline{U}_a$, wall thickness δ, and n lattice planes in δ may be written approximately as

$$U_{wall} = \overline{U}_a \delta + \frac{JS^2\pi^2}{a\delta}, \tag{26}$$

where a is the atomic lattice spacing. This relationship is valid only when rotation is uniform within the wall (so the anisotropy energy is independent of wall thickness), when the exchange energy of two parallel magnetic moments in Eq. (25) is set equal to 0, and when the spin quantum numbers S_i and S_j are the same. The cosine of the angle θ between the spin quantum numbers S_i and S_j is also expanded in a power series in θ. Terms higher than the second term are neglected.

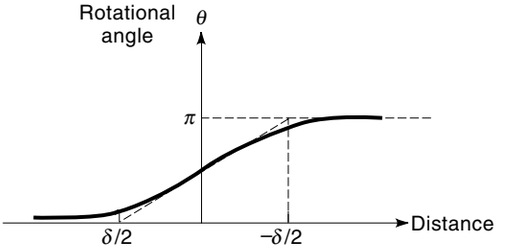

Figure 8. Nonuniform variation of rotational angle of magnetic moments across a Bloch domain wall as a function of distance from the center of the wall.

For a minimum in domain-wall energy, $\partial U_{\text{wall}}/\partial\delta = 0$, which yields the approximate relationship for evaluating domain wall thickness:

$$\delta = \left(\frac{JS^2\pi^2}{a\overline{U}_{\text{a}}}\right)^{1/2} \tag{27}$$

For a body-centered cubic iron crystal, Eq. (27) yields a domain-wall thickness that is approximately 0.04 μm or 146 base vectors of the lattice. In fact, the rotation of magnetic moments across a Bloch wall is not uniform but has the form given in Fig. 8.

The minimum energy state of a bulk ferromagnetic specimen is generally one of multi-domain formation. For very thin films, whose easy axis is along the film normal, domain structure is approximately parallel to the surface of the film in the main body of the film, and closure domains form at the edges of the film (3). As film thickness increases, however, planar multidomains and domains whose planes tilt away from the film surface form. The direction of magnetization in the domain wall of a thin film (whose thickness is much less than the domain-wall thickness) also changes from that of a Bloch wall, normal to the plane of the film, to that of a Néel wall (6), parallel to the surface of the film (see Fig. 9). This is energetically favorable because the surface energy associated with demagnetization in such a film is minimized. This is particular true for thin films of ferromagnetic materials that have negligible crystalline anisotropy, such as Permalloy. In general, the thickness of Bloch domain walls increases, whereas the thickness of Néel walls decreases with increasing film thickness. The domain-wall energy of Bloch walls, on the other hand, decreases with increasing film thickness and that of Néel walls increases.

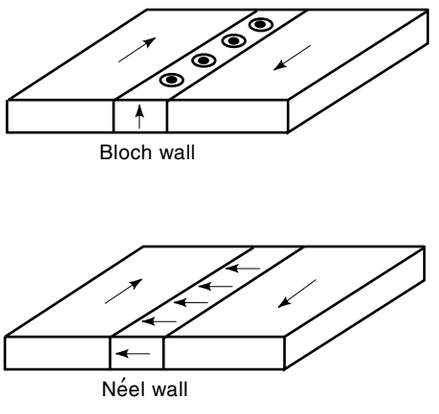

Figure 9. A Bloch wall and a Néel wall in a magnetic thin film (6).

Magnetostatic Energy. The magnetostatic energy of a specimen results from the effects of demagnetization and is highly shape-dependent. Equivalent magnetic poles occur at the intersection of a domain wall with the surface of the material and give rise to stray fields external to the specimen. These create an opposing general *demagnetizing field* $\boldsymbol{H}_{\text{D}}$ with orientation opposite to the polarization vector internal to the specimen. The energy associated with the demagnetizing field may be written

$$E_{\text{ms}} = -\frac{1}{2}\int_V \boldsymbol{M}\cdot\boldsymbol{H}_{\text{D}}\,dv \tag{28}$$

Minimization of magnetostatic energy in bulk materials increases the number of domains until the decrease of magnetostatic energy associated with domain growth is compensated for by the increased energy of the Bloch walls. This gives a net minimum in energy. For magnetocrystalline anisotropy that has cubic symmetry, there are special domain configurations in which no external fields are created because adjacent domains may produce equal and opposite equivalent magnetic mass densities. In a thin film the configuration of the magnetization vector in the domain wall changes from that of a Bloch wall to a Néel wall or a *cross-tie* wall (3) to mimimize surface regions that would have high demagnetization energies.

Magnetostriction Energy

Magnetostriction energy is the elastic energy associated with the dimensional change in a specimen resulting from magnetic polarization between neighboring domains. Magnetostriction occurs because of anisotropy. Magnetostrictive expansion or contraction of a crystalline lattice during the magnetization process is the reaction of the lattice to rotation of the magnetization vector from easy to hard directions. A material has positive magnetostriction if a specimen expands in the direction of the magnetization and negative magnetostriction if it contracts in the direction of magnetization. Hence, this energy varies according to the structure of the domains. Magnetostriction deforms domain configuration so as to minimize magnetostrictive energy. Magnetostriction energy is defined as the work necessary to reassemble domains to their initial states.

MAGNETIC SWITCHING ANALYSIS

Magnetic switching depends strongly on the dynamics, or the time dependence, of the process. The timescales required for magnetic switching cover a wide range. Magnetization reversal processes in some applications are on the order of seconds, while others are on the order of 10 ns or less. Switching speeds are limited by both eddy currents and by the intrinsic or relaxation damping mechanisms. Because of the wide timescales, the process of magnetic reversal can be studied either by seeking information about the final equilibrium position of the magnetization vector at a given point in the material without determining the details of the magnetization

process before equilibrium is attained or by following the position of the magnetization vector as a function of time during the magnetization reversal process. The approach followed depends on the application, but the second approach is more complex. The analysis for both approaches is outlined and discussed.

Thin metallic films represent the principal media for present-day high density magnetic recording. They are prominent examples of dynamic, fast magnetic switching applications. Hence we refer here mostly to thin films. The films of Permalloy ($Ni_{81}Fe_{19}$) are widely used in manufacturing more than one billion recording heads annually.

In the process of magnetic recording, information must first be stored on special magnetic media. Next, this information must be retrieved by reading the information stored on the media. Both the writing and reading are strongly tied to the magnetic switching process and to the relevant properties of the medium. During writing, the magnetization of the medium has to be locally switched from the well-defined orientation corresponding to the negative remanent state to the well-defined positive remanent state. These two magnetization states may be represented by "0" or "1" to store information on the binary system. The dimensions of the switched area are usually on the order of micrometers that have submicrometer separation between magnetization states. For example, the transition spacing between oppositely magnetized regions on present-day hard disk drives is about 0.2 μm, and track periods are on the order of 3 μm to 4 μm. Future applications will have even smaller transition spacings. To decrease noise, the switched area should have sharp boundaries and be stable with time, while allowing complete erasure. All of these parameters define the properties of the recording medium and the writing head. In reference to the switching process, they determine the amplitude of the bias field necessary to reverse the position of the magnetization, or the so-called *switching field,* and the *switching time.* The switching time is the time needed to reverse the magnetization position that uniquely defines the desired state.

During reading, the reading head moves above the recorded signal, and the response to the presence of the 0 or 1 state is monitored. Formerly, recording heads were inductive, and the response of the head corresponded to the voltage induced in a coil coupled to the magnetic structure. More recently, these heads have been replaced by *magnetoresistive* heads, whose response is proportional to the change in electrical resistivity of the head in a magnetic field. This change in resistivity occurs as the head moves over the recorded information. Other reasons for using magnetoresistive heads are not discussed here. What is important is the fact that the resistivity of the head depends on the strength and orientation of the magnetic field produced by the orientation of the magnetization on the recording medium. The first resistive reading heads were based on the effect of anisotropic magnetoresistance (AMR). The resistivity depends on the relative orientation of the current I through the film with respect to the direction of the magnetization M in the film. For Permalloy films deposited on silicon wafers, the resistivity at room temperature with M parallel to I is about 2.5% larger than when M is perpendicular to I.

Giant Magnetoresistance

The possibility for significantly enhancing the sensitivity and dynamic range of recording magnetoresistive heads resulted from the discovery of the giant magnetoresistance (GMR) in coupled iron-chromium layered structures (7,8). GMR is characteristic of electric current behavior in materials consisting of alternating ferromagnetic and nonmagnetic layers of ferromagnetic and nonmagnetic metals deposited on an insulating substrate. The resistance, measured with current flowing parallel to the layers, is greater when the magnetic moments in the alternating ferromagnetic layers are oppositely aligned

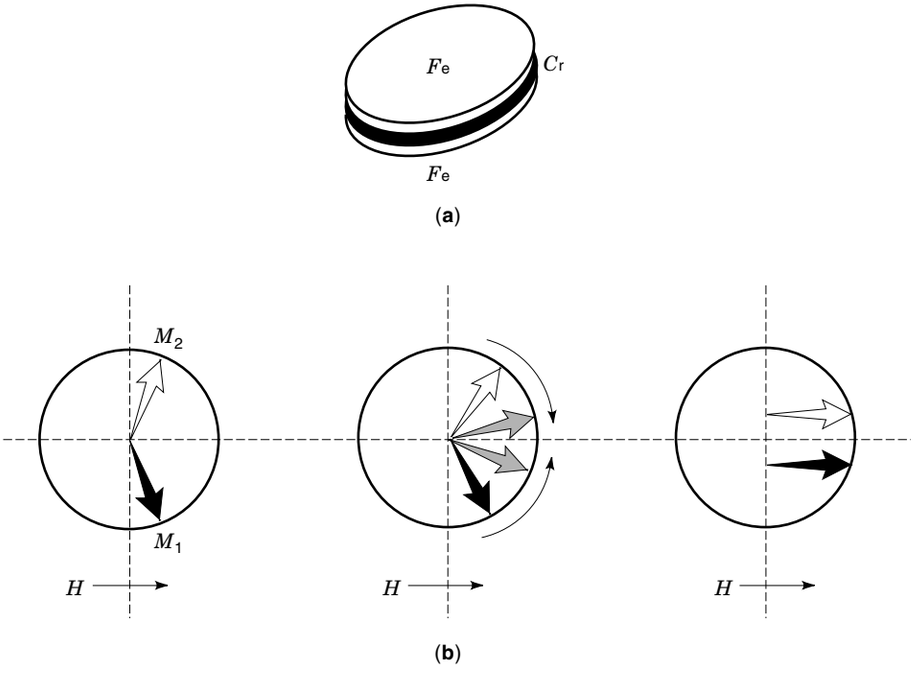

Figure 10. Giant magnetoresistive Fe/Cr layered structures (a) and possible equilibrium positions of magnetic moments for several applied fields $\boldsymbol{H}$ (b).

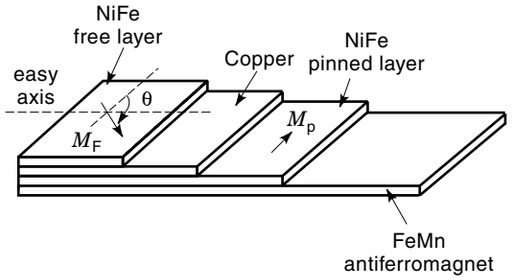

Figure 11. Structure of spin valve showing two uncoupled ferromagnetic films separated by a nonmagnetic metal layer. The bottom film is pinned.

and smallest when they are all parallel. The measured relative change in resistivity can be several hundred percent at low temperatures. The structure is shown for two single-domain layers in Fig. 10. Figure 10 also shows possible equilibrium positions of the layers' magnetic moments for several applied fields. In contrast with AMR, GMR depends only on the relative orientation θ of the magnetic moments of the layers. GMR results from spin-dependent scattering of the conductive electrons at the interfaces and may be expressed as

$$R = R_0 - \frac{\Delta R}{2}(\cos\theta + 1) \tag{29}$$

where R_0 is the resistivity in zero field ($H = 0$), and ΔR is the maximum difference in resistivity corresponding to the parallel and antiparallel orientation of moments. Even larger effects are observed in a perpendicular geometry where the current flows perpendicular to the layers. GMR has also been observed in heterogeneous alloys and granular multilayers.

Spin Valve. The magnetoresistance of GMR structures increases with the number of alternating layers. This, however, complicates mass production and could decrease manufacturing yield. One question is whether it is possible to find a combination that allows GMR behavior and to make a more simple head structure. One of the solutions that fulfills these criteria is the *spin valve* (9). The schematic structure of the spin valve is shown in Fig. 11. A spin valve consists of just two uncoupled ferromagnetic films (Permalloy or cobalt) separated by a nonmagnetic metal layer (copper, silver, gold) spacer. The magnetization of one layer is pinned through exchange coupling with an underlying antiferromagnet (iron manganese) in a specific direction. Like GMR structures, the resistance of the spin valve is proportional to the angle between the magnetic moments in the magnetic layers. Because the ferromagnetic layers are only weakly coupled, the magnetization of the free layer is easy to rotate relative to the pinned layer, making the spin valve sensitive to low fields.

The previous examples demonstrate that a clear understanding of the magnetization reversal process is requisite to optimize heads for recording applications. In the following sections we outline the essential features of the magnetic switching process. The analysis is performed in two steps. First, only the quasi-static magnetization reversal is considered. Second, the more complex problems of dynamic switching are discussed.

Quasi-static Magnetization Reversal

Single-Domain Particle Behavior. Many models have been employed to explain hysteresis properties of single-domain particles (10). These models may be classified into those in which the particle reverses its magnetization in the single-domain state (coherent rotation) and those in which the magnetization does not remain uniformly parallel during the switch (incoherent rotation). The single-domain particle remains physically fixed during these rotations. Only the magnetization changes direction. The classical model of Stoner–Wohlfarth (11) involves only coherent rotation. Although this model does not completely apply to even single-domain particles, it provides an important understanding of magnetic switching and of more complicated models of the magnetization reversal process. It also permits systematic introduction of the necessary terms describing magnetic switching.

In static equilibrium, the torque on the magnetization exerted by the total magnetic field must vanish at every point in the medium, that is,

$$\boldsymbol{M} \times \boldsymbol{H}_{\text{eff}} = 0 \tag{30}$$

where the effective magnetic field consists of the external applied magnetic field $\boldsymbol{H}_0$, a magnetic field due to the magnetization of the medium, the magnetostatic or demagnetizing field $\boldsymbol{H}_D$, the magnetic anisotropy field $\boldsymbol{H}_a$, and the magnetic exchange field $\boldsymbol{H}_{ex}$.

Assume a single-domain particle in the form of a thin film as portrayed in Fig. 12, where the saturation magnetization of the particle is M_s and where $\boldsymbol{M}$ is tilted from the z-axis by an angle θ_0 with an applied bias field $\boldsymbol{H}_0$ in the y-direction. If the particle has a preferred direction of magnetization along the z-axis, the minimum energy state is obtained in this *easy* direction. In such a uniaxial material, any deviation of $\boldsymbol{M}$ away from the easy axis by an angle θ leads to an increase of the energy. When $\boldsymbol{M}$ is inclined by an angle θ to the easy axis, the anisotropy field can be simply interpreted as the magnetic field H_a appearing perpendicular to the easy axis that is opposed to the component of $\boldsymbol{M}$ in this direction. This may be expressed mathematically by

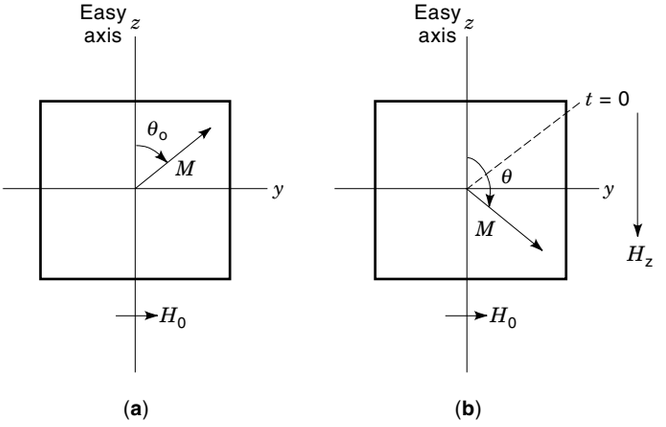

Figure 12. A single-domain particle in the form of a thin film. $\boldsymbol{M}$ is magnetization and $\boldsymbol{H}_0$ is the applied field.

$$\boldsymbol{H}_{\mathrm{a}} = -\frac{1}{M_{\mathrm{s}}} \nabla_{\alpha} E_{\mathrm{a}}|_{\alpha_{\mathrm{eq}}} \tag{31}$$

where M_{s} is the saturation magnetization of the material and the gradient of the anisotropy energy E_{a} is evaluated at the equilibrium position. The z-component of the anisotropy field in a uniaxial material may be written directly from Eq. (31) as

$$H_{\mathrm{az}} = \frac{2K_{\mathrm{u}}}{M_{\mathrm{s}}} \cos\theta = H_{\mathrm{a}} \cos\theta \tag{32}$$

When a switching field H_{z} is applied (Fig. 12), the static equilibrium condition expressed by Eq. (30) gives the following relationship between θ and the magnetic field H_{z}:

$$H_{\mathrm{z}} = -H_{\mathrm{a}}(\cos\theta - \sin\theta_0 \cot\theta) \tag{33}$$

A plot of $M_{\mathrm{z}}/M_{\mathrm{s}}$ versus $H_{\mathrm{z}}/H_{\mathrm{a}}$ in Fig. 13 shows the quasi-static magnetization characteristic of a single-domain particle when pure rotation of the magnetization takes place. Even for this simple case of magnetic reversal by uniform rotation, magnetic hysteresis is evident. In other words, decreasing or increasing the applied field does not necessarily lead to the same magnetic state. The field H_0 in Fig. 13 was chosen arbitrarily so that $\theta_0 = 30°$. Magnetic switching of the particle must occur when $\theta \geq \theta_{\mathrm{c}}$, at which point $dH_{\mathrm{z}}/d\theta = 0$. From Eq. (33)

$$\sin^3\theta_{\mathrm{c}} = \sin\theta_0 \tag{34}$$

and

$$\cos^3\theta_{\mathrm{c}} = \frac{H_{\mathrm{zc}}}{H_{\mathrm{a}}} \tag{35}$$

A plot of H_{zc} versus H_0 is usually known as the *switching asteroid* that has a minimum critical switching field for $\theta_0 = 45°$. The previous results are also obtained from energy considerations. The free energy density of the single-domain particle in Fig. 12(b) is given by

$$E_0 = K_{\mathrm{u}} \sin^2\theta_0 + M_{\mathrm{s}} H_0 \sin\theta_0 \tag{36}$$

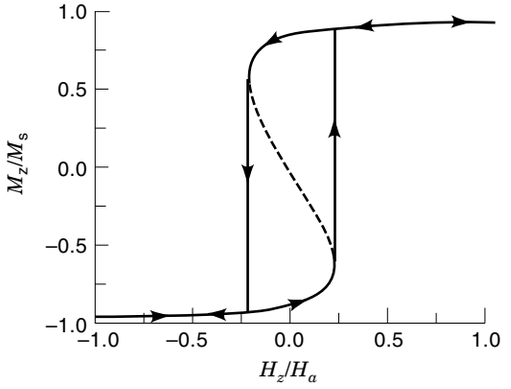

Figure 13. Hysteresis plot of $M_{\mathrm{z}}/M_{\mathrm{s}}$ versus $H_{\mathrm{z}}/H_{\mathrm{a}}$ showing the quasi-static magnetization characteristic of a single-domain particle in uniform rotation.

for the initial state and

$$E = K_{\mathrm{u}} \sin^2\theta + M_{\mathrm{s}} H_0 \sin\theta - M_{\mathrm{s}} H_{\mathrm{z}} \cos\theta \tag{37}$$

for the final state. The equilibrium condition is obtained at a (local) minimum of the free energy with respect to the angles θ and θ_0, that is, $\partial E/\partial\theta = 0$ and $\partial E/\partial\theta_0 = 0$. The latter equilibrium conditions yield Eq. (33).

In general, for single-domain particles, the lowest energy eigenmodes of magnetic reversal are sought. For ellipsoids of revolution, these are either the *fanning* modes of coherent rotation or the *curling* and *buckling* modes of incoherent rotation (10). The fanning modes are named from the model of individual domains of equal volume spheres forming chains, where the magnetization vector in each sphere rotates in a direction alternate from its neighbor. Recent measurements of the angular dependence of the switching field in single-domain ferromagnetic particles (12), however, show that switching generally differs from the uniform rotational model. Both measurement data and analysis indicate that switching is represented by curling modes for $\theta \sim 0°$. For $\theta > 30°$, switching agrees closely with the coherent rotational model previously described. Incoherent reversal is usually thought to occur as a result of inhomogeneities in the particles, such as grain boundaries, voids, dislocations, cracks, and mechanical strains.

Multiple-Domain Particle Behavior. In multiple-domain particles the reversal process occurs through domain-wall motion that consists of both rotation in unison and "incoherent" rotation. The incoherent rotation depends on the magnitudes of both the switching and biasing fields. The quasi-static magnetization characteristics of reversal in this case are not unlike the hysteresis shown for the single-domain particle in Fig. 13. Ferromagnetic hysteresis has its origin, as illustrated by the previous simple analysis, in the multiplicity of metastable states in the system's free energy. This very general statement is difficult to quantify for predictive use. Just as difficult is the task of following the behavior of each domain and domain wall during the reversal process at each spatial position of the specimen—even for quasi-static treatment. Hence a more viable approach pursued by many researchers is based on phenomenological models in which all essential hysteresis characteristics are obtained as a direct consequence of a few, simple, initial assumptions. These assumptions are usually not concerned with the details of the magnetic state at a given point in the specimen nor are they concerned with the details of the domain walls and structure. Instead, they rely on a set of experimental data, collectively called an *identification process,* to determine a few constants relating a specific model to the specimen that permit predicting magnetic material behavior as a function of the applied magnetic field in a given direction.

Among the most widely known models are the Preisach (13) and the Williams–Comstock (14). The Preisach model was later extended by DelaTorre (15,16), Mayergoyz (17), and Jiles and Atherton (18). In the Preisach model, hysteresis is described by a collection of a large number of elementary reversible λ_{α} and irreversible $\gamma_{\alpha\beta}$ bistable units (see Fig. 14), each characterized by the values α and β, $\alpha > \beta$, at which the external field H_0 makes the unit switch up or down. The bistable unit $\gamma_{\alpha\beta}$ can be considered a quasi-domain that switches

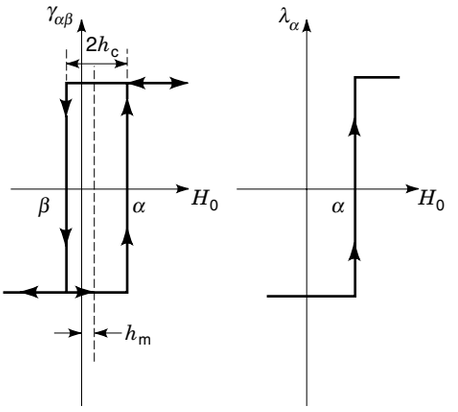

Figure 14. Preisach model of hysteresis described by a collection of elementary reversible λ_α and irreversible $\gamma_{\alpha\beta}$ bistable units.

with increasing applied field from the state $-M_s$ to the state $+M_s$ at the field α. With a decreasing applied field, the bistable unit reverses from the $+M_s$ to the $-M_s$ state at the field value β. For such a quasi-domain a local coercivity (switching field) $h_c = (\alpha - \beta)/2$ and an effective field from the neighboring quasi-domains $h_m = (\alpha + \beta)/2$ correspond. For $\beta < H_0 < \alpha$, $\gamma_{\alpha\beta}$ depends on the previous state of the specimen. Then a system of multidomain particles is described by the switching distributions $p(\alpha, \beta)$ and $\nu(\alpha)$, and the magnetization is expressed as

$$M(t) = \int_\alpha \int_\beta p[\alpha, \beta, H_0(t)]\gamma_{\alpha\beta}[H_0(t)]\,d\alpha\,d\beta + \int_{-\infty}^{\infty} v(\alpha)\lambda_\alpha[H_0(t)]\,d\alpha \tag{38}$$

Although Eq. (38) contains time-dependent variables, nonetheless the model is static and does not take into account the speed at which magnetization changes. The time-dependent magnetization corresponds to a step-by-step field change, but the output is still a sequence of equilibrium states that depend only on the value of the field H_0. Mayergoyz (17) proved that a system with hysteresis is equivalent to the Preisach model if it obeys the "wiping out or return-point memory" and "congruency or geometrical equality" properties. The first condition means that each local maximum H_{0m} field value wipes out the influence of the previous local maxima. The congruency property that defines the geometric equivalence of all minor loops delimited by the same peak field values has not been verified for real systems. Experimentally observed minor hysteresis loops become smaller when remanence is approached. However, this defect in the second condition is eliminated if a feedback correction to H_0 is added which produces an internal effective field H_i:

$$H_i = H_0 + CM \tag{39}$$

As the constant C becomes larger, the hysteresis loop becomes more rectangular or the squareness ratio defined by M_r/M_s in Fig. 7 becomes closer to one. The squareness ratio depends on the ratio of the average magnetostriction constant to the first-order anisotropy constant. A smaller ratio of the magnetostriction constant to the first-order anisotropy constant yields more hysteresis-loop squareness. The completely reversible magnetization process is given by the second term in Eq. (38).

Dynamic Magnetization Reversal

The quasi-static models describing magnetic reversal do not give the system's time response straightforwardly, especially for fast switching processes. A different approach is necessary to calculate the fast magnetization switching response at an arbitrary time and at each point of the recording medium. All forces acting on the magnetization at any point in space on the recording medium and at any time must be used to characterize the complete magnetization reversal. In general, it is assumed that the direction cosines and the magnitude of the magnetization vector vary continuously with position. Depending on the actual problem, changes may vary on a scale that is smaller or comparable to the domain size. This type of treatment forms the foundation of the micromagnetic modeling approach advocated by Brown (2).

Here a procedure based on the Landau–Lifshitz equation is followed (19). Landau and Lifshitz first introduced the phenomenological representation of the interactive forces with an effective internal field $\boldsymbol{H}_{\text{eff}}$. The action of this field is equivalent to the applied field but also includes other interactions in the ferromagnetic material. Generally, the magnetization becomes parallel to the effective field. Therefore Landau and Lifshitz next proposed an ad hoc damping term into the magnetization equation of motion which has the direction of $\boldsymbol{H}_{\text{eff}} - \boldsymbol{M}$ and an amplitude that approaches 0 when $\boldsymbol{H}_{\text{eff}}$ and $\boldsymbol{M}$ become parallel. The Landau–Lifshitz equation, which conserves total magnetization, can be written as

$$\frac{d\boldsymbol{M}}{dt} = -|\gamma|(\boldsymbol{M} \times \boldsymbol{H}_{\text{eff}}) + \boldsymbol{R} \tag{40}$$

where the specific forms of the damping term $\boldsymbol{R}$ most used are

$$\boldsymbol{R} = |\gamma|\lambda\left[\boldsymbol{H}_{\text{eff}} - (\boldsymbol{H}_{\text{eff}} \cdot \boldsymbol{M})\frac{\boldsymbol{M}}{M_s^2}\right] \tag{41}$$

$$\boldsymbol{R} = -\frac{\alpha|\gamma|}{M_s}(\boldsymbol{M} \times \boldsymbol{M} \times \boldsymbol{H}_{\text{eff}}) \tag{42}$$

and

$$\boldsymbol{R} = \frac{\alpha}{M_s}\left(\boldsymbol{M} \times \frac{d\boldsymbol{M}}{dt}\right) \tag{43}$$

Equation (43) is known as the Gilbert damping form. λ is the damping parameter that has the dimension of magnetization. The dimensionless Gilbert damping parameter $\alpha = \lambda/M_s$.

Now the effective field $\boldsymbol{H}_{\text{eff}}$, which represents all interactions, is introduced. If the free energy of the system is evaluated by the variational principle, the amplitude and direction of the internal field can be determined with good approximation. However, the resulting form is too general, and it is more practical to express the effective field as the power series:

$$\begin{aligned}\boldsymbol{H}_{\text{eff}}(\boldsymbol{M}) &= -\frac{\partial E}{\partial \boldsymbol{M}} + \sum_i^3 \frac{\partial}{\partial x_i}\left[\frac{\partial E}{\partial(\partial \boldsymbol{M}/\partial x_i)}\right] \\ &= \boldsymbol{H}_0(t) + \boldsymbol{H}_a(\boldsymbol{M}) + \boldsymbol{H}_D(\boldsymbol{M}) + \boldsymbol{H}_{ex}(\boldsymbol{M})\end{aligned} \tag{44}$$

The $\boldsymbol{H}_0$ and $\boldsymbol{H}_a$ terms of Eq. (44) are the time-dependent applied field and the anisotropy field. The term $\boldsymbol{H}_D(\boldsymbol{M})$ represents the demagnetizing field of the specimen [see also Eqs. (15, 16)], which is solved by Maxwell's equations for the particular specimen shape of interest, that is,

$$\begin{aligned} \nabla \cdot [\boldsymbol{H}_D(\boldsymbol{r}, t) + \boldsymbol{M}(\boldsymbol{r}, t)] &= 0 \\ \nabla \times \boldsymbol{H}_D(\boldsymbol{r}, t) &= 0 \end{aligned} \tag{45}$$

For the quasi-static case, this set of equations leads to the Poisson equation, and, for a specimen that has the shape of an ellipsoid of revolution, the solution for $\boldsymbol{H}_D$ can be expressed in terms of the demagnetizing tensor $[N]$. If the specimen is magnetized along one of its principal axes, the tensor is diagonal with the individual components N_x, N_y, and N_z satisfying the condition $\sum_i^3 N_i = 1$. The ensuing solution for $\boldsymbol{H}_D$ is given by

$$\boldsymbol{H}_D(\boldsymbol{r}) = \frac{1}{4\pi} \nabla \left(\int_V \frac{\nabla \cdot \boldsymbol{M}}{r} dV + \int_S \frac{\boldsymbol{M} \cdot \boldsymbol{n}}{r} dS \right) \tag{46}$$

The first integral is taken over the entire volume of the magnetized specimen, the second integral over the enclosing surface of the magnetized specimen, and the unit normal vector $\boldsymbol{n}$ to the surface is directed inward.

The last term in Eq. (44) is the exchange field which quantifies the quantum mechanical exchange interactions between neighboring spins:

$$\boldsymbol{H}_{ex}(\boldsymbol{M}) = \frac{G}{M_s} \nabla^2 \boldsymbol{M}(\boldsymbol{r}, t) \tag{47}$$

where $G = 4JS^2/(aM_s) = 2A/M_s$ is the exchange parameter, J is the exchange energy integral, S is the spin quantum number, a the lattice constant of the magnetic unit cell, and $A = 2JS^2/a$ ranges between 10^{-11} and 10^{-12} J/m.

One example that gives insight into the dynamic switching process is the uniform rotation of magnetization in a thin film. The procedure is outlined by Soohoo (20). For coherent rotation in a single-domain particle, magnetization does not depend on position in the specimen, so that the analysis is considerably simplified. However, the magnetization is a function of both azimuthal and polar angles (see Fig. 15). The effective field in Eq. (44) may be expressed in terms of the free energy and its derivatives. If the Gilbert modification of the Landau–Lifshitz equation is expressed in spherical coordinates,

$$M_s \frac{d\theta}{dt} = \frac{-|\gamma|}{\sin\theta} \frac{\partial E}{\partial \phi} - \alpha M_s \sin\theta \frac{d\phi}{dt}$$

and

$$M_s \sin\theta \frac{d\phi}{dt} = |\gamma| \frac{\partial E}{\partial \theta} + \alpha M_s \frac{d\theta}{dt} \tag{48}$$

Now the dynamic behavior of the magnetization is obtained by numerically solving the two coupled differential Eqs. (48) as a function of θ and ϕ. Standard numerical techniques, such as the Euler and Runge–Kutta-type methods or predictor-corrector methods (21) may be employed. For sufficiently small switching speeds, $\partial\phi/dt \sim 0$ and the switching time $(\Delta t)_s$ can be written from the second of Eqs. (48) as

$$(\Delta t)_s = -\frac{\alpha M_s}{|\gamma|} \int_{\theta_i}^{\theta_f} \frac{d\theta}{\partial E/\partial\theta} \tag{49}$$

where θ_i and θ_f are the initial and final orientations of the magnetization.

Two significant differences are apparent when comparing quasi-static reversal analysis to dynamic analysis. The first difference is that the switching time depends on the damping constant of the system and on the time-dependent torque acting on the magnetization during its entire reversal. The second difference is that even in the simplest case of single-domain uniform rotation, the motion of magnetization is more complicated and *is not confined to the plane of the film.* Because the torque $\boldsymbol{M} \times \boldsymbol{H}_{eff}$ for uniform rotation of a single-domain is directed out of the plane of the film, in the process of rotation the magnetization $\boldsymbol{M}$ tips slightly out of the plane of the film. This gives rise to an x-component ΔM_x and an accompanying demagnetizing field $H_{Dx} \simeq N_x \Delta M_x$. The demagnetizing field, in turn, exerts a torque on the magnetization in the plane of the film so as to rotate the magnetization toward the negative z-axis. The previous analysis is simplified and does not predict switching times observed experimentally. However, it gives proper insight into the general switching process. The discrepancy between calculated switching times from Eq. (49) and experimentally observed times is attributed to an incorrect assumption of a position-independent magnetization. In fact, thin films have initial magnetization ripples, and the magnetostatic field originating from $\nabla \cdot \boldsymbol{M}$ of the ripple distribution plays a significant part in the reversal process (22–24).

In this article we investigated the simple case of the dynamic behavior of a single-domain particle in a thin ferromagnetic film. Recent technological applications involve magnetic systems of much greater complexity. These systems possess complicated geometries and have nonuniform demagnetizing fields within multidomain particles, which leads to highly nonuniform distributions of the magnetization within the particles. The Landau–Lifshitz equation expressing damping is used almost exclusively to calculate the dynamics of polycrystalline, thin-film recording media and thin metallic films. It is also used to calculate the dynamic micromagnetics of submicrometer ferromagnetic particles.

The analysis of more complex systems can be the same as that outlined. In principle, the Landau–Lifshitz equation can

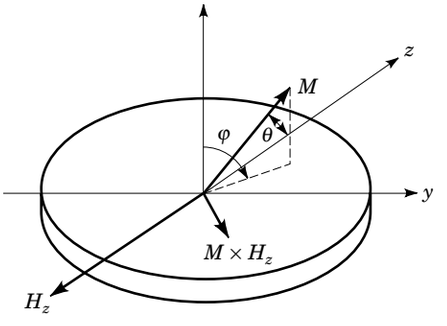

Figure 15. Rotation of magnetization as a function of azimuthal and polar angles in a thin film, where z represents the easy axis and the vertical line is x.

be solved for a continuous magnetic medium in three-dimensional regions of arbitrary geometry and arbitrary properties for nanosecond time-dependent processes. All interactions, based on calculating the effective field from free energy system considerations, are included in the micromagnetic approach. The magnetic specimen can be discretized and the magnetization as well as the acting effective fields can be taken as position-dependent (spatially inhomogeneous). Then appropriate boundary conditions may be applied. Computational times for the analysis depend on the number of cells used in the model. For some cases, computational time is reduced by assuming that the magnetization in each cell is uniform and that the switching process in the cell is described by pure rotation. Numerical simulations of the dynamic process reveal that the magnetization switching process is divided into three stages that are not significantly different from the micromagnetic calculations outlined previously or from experimental data: (1) precursor nucleation process (critical field or coercive field for magnetization reversal); (2) magnetization curling (incoherent rotation); and (3) actual switching and damping.

During the first stage, the motion of magnetization is almost stationary, and precession occurs along the equilibrium direction. If the switching field is less than critical, the magnetization settles in the equilibrium position without switching. In the curling stage, the magnetization along the applied magnetic field direction increases exponentially. For an ellipsoid of revolution, the curling starts from the center of the ellipsoid and extends from this center with time. Parts of the specimen switch first. This results in the appearance of domain walls and subsequent events that depend on both the damping and switching field, such as the generation of vortices (25–28). Additional complexity can be introduced in the model by taking into account possible random orientation of the crystalline anisotropic axes and interactions between neighboring cells. The same analytic procedures apply.

BIBLIOGRAPHY

1. P. Weiss, L'hypothese du champ moleculaire et la propriete ferromagnetique, *J. Phys. Theor. Appl.* 4E, **series 6**: 661, 1907.
2. W. F. Brown, Jr., *Micromagnetics,* New York: Interscience Publishers, 1963.
3. R. F. Soohoo, *Magnetic Thin Films,* New York: Harper and Row, 1965.
4. N. S. Akulov, Magnetostriction in iron crystals, *Z. Physik,* **52**: 389–405, 1928.
5. N. S. Akulov, *Ferromagnetism,* Moscow and Leningrad: ONTI, 1939.
6. C. Kittel, *Introduction to Solid State Physics,* New York: Wiley, 1986.
7. M. N. Baibich et al., Giant magnetoresistance of (001)Fe/(001)Cr magnetic superlattices, *Phys. Rev. Lett.,* **61**: 2472–2475, 1988.
8. P. Grünberg et al., Layered magnetic structures: Evidence for antiferromagnetic coupling of Fe layers across Cr interlayers, *Phys. Rev. Lett.,* **57**: 2442–2445, 1986.
9. B. Dieny et al., Magnetotransport properties of magnetically soft spin-valve structures, *J. Appl. Phys.,* **69**: 4774–4779, 1991.
10. J. C. Mallinson, *The Foundations of Magnetic Recording,* New York: Academic Press, 1993.
11. E. C. Stoner and E. P. Wohlfarth, A mechanism of magnetic hysteresis in heterogeneous alloys, *Phil. Trans. R. Soc. London A,* **240**: 599–642, 1948.
12. M. Lederman, S. Schultz, and M. Ozaki, Measurement of the dynamics of the magnetization reversal in individual single-domain ferromagnetic particles, *Phys. Rev. Lett.,* **73**: 1986–1989, 1994.
13. F. Preisach, Über magnetische Nachwirkung, *Z. Physik,* **94**: 277–302, 1935.
14. M. L. Williams and R. L. Comstock, An analytical model of the write process in digital magnetic recording, *17th Annu. AIP Conf. Proc.,* Chicago, IL, 1971, pp. 738–742.
15. E. Della Torre, Effect of interaction on the magnetization of single domain particles, *IEEE Trans. Audio Electroacoust.,* **14**: 86–93, 1966.
16. F. Vajda, E. Della Torre, and M. Pardavi-Horvath, Analysis of reversible magnetization-dependent Preisach models for recording media, *J. Magn. Magn. Materials,* **115**: 187–189, 1992.
17. I. D. Mayergoyz, Mathematical models of hysteresis, *Phys. Rev. Lett.,* **56**: 1518–1521, 1986.
18. D. C. Jiles and D. L. Atherton, Theory of ferromagnetic hysteresis, *J. Magn. Magn. Matter,* **61**: 48–60, 1986.
19. L. Landau and E. Lifhshitz, On the theory of the dispersion of magnetic permeability in ferromagnetic bodies, *Phys. Z. Sowjetunion,* **8** (2): 153–169, 1935.
20. R. F. Soohoo, *Theory and Application of Ferrites,* Englewood Cliffs, NJ: Prentice-Hall, 1960.
21. G. A. Korn and T. M. Korn, *Mathematical Handbook for Scientists and Engineers,* New York: McGraw-Hill, 1968.
22. M. H. Kryder and F. B. Humphrey, Dynamic Kerr observations of high-speed flux reversal and relaxation processes in permalloy thin films, *J. Appl. Phys.,* **40**: 2469–2474, 1969.
23. M. H. Kryder and F. B. Humphrey, Mechanisms of reversal with bias fields, deduced from dynamic magnetization configuration photographs of thin films, *J. Appl. Phys.,* **41**: 1130–1138, 1970.
24. H. Hoffmann and M. H. Kryder, Blocking and locking during rotational magnetization reversal in ferromagnetic thin films, *IEEE Trans. Magn.,* **9**: 554–558, 1973.
25. B. Yang and D. R. Fredkin, Dynamical magnetics of a ferromagnetic particle: Numerical studies, *J. Appl. Phys.,* **79**: 5755–5757, 1996.
26. Q. Peng and H. N. Bertram, Micromagnetic studies of switching speed in longitudinal and perpendicular polycrystalline thin film recording media, *J. Appl. Phys.,* **81**: 4384–4386, 1997.
27. J.-G. Zhu, Y. Zheng, and X. Lin, Micromagnetics of small size patterned exchange biased Permalloy film elements, *J. Appl. Phys.,* **81**: 4336–4341, 1997.
28. Y. Zheng and J.-G. Zhu, Switching field variation in patterned submicron magnetic film elements, *J. Appl. Phys.,* **81**: 5471–5473, 1997.

RICHARD G. GEYER
National Institute of Standards and Technology

PAVEL KABOS
Colorado State University